C_6 coefficients for interacting Rydberg atoms and alkali-metal dimers

Vanessa Olaya,[1] Jesús Pérez-Ríos,[2] and Felipe Herrera[1,3,*]

[1]*Department of Physics, Universidad de Santiago de Chile, Avenida Ecuador 3493, Santiago, Chile*
[2]*Fritz-Haber-Institut der Max-Planck-Gesellschaft, Faradayweg 4-6, 14195 Berlin, Germany*
[3]*Millennium Institute for Research in Optics (MIRO), Concepción, Chile*

(Received 31 December 2019; revised manuscript received 25 February 2020; accepted 28 February 2020; published 23 March 2020)

We study the van der Waals interaction between Rydberg alkali-metal atoms with fine structure (n^2L_j; $L \leqslant 2$) and heteronuclear alkali-metal dimers in the ground rovibrational state ($X\ ^1\Sigma^+$; $v = 0$, $J = 0$). We compute the associated C_6 dispersion coefficients of atom-molecule pairs involving ^{133}Cs and ^{85}Rb atoms interacting with KRb, LiCs, LiRb, and RbCs molecules. The obtained dispersion coefficients can be accurately fitted to a state-dependent polynomial $O(n^7)$ over the range of principal quantum numbers $40 \leqslant n \leqslant 150$. For all atom-molecule pairs considered, Rydberg states $n\,^2S_j$ and $n\,^2P_j$ result in attractive $1/R^6$ potentials. In contrast, $n\,^2D_j$ states can give rise to repulsive potentials for specific atom-molecule pairs. The interaction energy at the LeRoy distance approximately scales as n^{-5} for $n > 40$. For intermediate values of $n \lesssim 40$, both repulsive and attractive interaction energies of the order of 10–1000 μK can be achieved with specific atomic and molecular species. The accuracy of the reported C_6 coefficients is limited by the quality of the atomic quantum defects, with relative errors $\Delta C_6/C_6$ estimated to be no greater than 1% on average.

DOI: 10.1103/PhysRevA.101.032705

I. INTRODUCTION

Rydberg atoms with high principal quantum number have exaggerated properties such as orbital sizes of thousands of Bohr radii, long radiative lifetime exceeding microseconds, and extreme sensitivity to static electric fields. The latter is due to their giant dipole moment and electric polarizability. These exotic features have made Rydberg atoms a widely studied platform for fundamental studies and applications such as quantum information processing [1], quantum nonlinear optics [2], and precision measurements [3]. There is a growing interest in the preparation and study of ultralong-range Rydberg molecules [4–7], which emerges from the binding of an alkali-metal atom to a Rydberg atom as a consequence of the elastic collisions of the Rydberg electron with the alkali-metal atom, and may lead to promising applications [8,9].

Ultracold Rydberg atoms can be trapped with high densities [10], enabling studies of strong long-range interactions [11,12] and many-body physics [13–15]. Rydberg atoms can resonantly exchange their excitation energy via Foster processes [16], which has been exploited in studies of gas-phase energy transfer [17] and the formation of ultracold plasmas [18–20]. Rydberg atoms can also exchange excitation energy in the microwave regime with molecular gases via Foster processes, which has been proposed as a tool for the nondestructive detection of molecular states in hybrid molecule-Rydberg systems [21,22]. Simultaneous trapping of ultracold Rydberg atoms and polar molecules may also be used for direct sympathetic cooling of molecules intro the ultracold regime—a longstanding goal in ultracold physics—through elastic van der Waals atom-molecule collisions [23,24]. In comparison with dipole-dipole processes, van der Waals collisions do not require molecules to be confined in low-dimensional traps in the presence of static electric fields for shielding detrimental attractive collisions that lead to trap loss [25]. Moreover, van der Waals interactions can be strong even if the relevant transition energies in the collision partners are not resonant, as opposed to Foster processes. Understanding the feasibility of these promising applications of molecule-Rydberg systems requires an accurate knowledge of the van der Waals interaction potentials.

For an atom-molecule system at low kinetic energies, the relevant scattering properties at distances beyond the LeRoy radius [26] are determined by the long-range interaction between particles [4]. For R being the distance between the center of mass of the molecule and the atom, the long-range interaction potential can be written as an expansion of the form $V(R) = \sum_n C_n/R^n$, with $n \geqslant 3$ for neutral particles. Since we consider atom-molecule interactions for molecules in their rovibrational ground state ($J = 0$), the lowest nonvanishing van der Waals coefficient is C_6 [27–29]. Dipole-dipole contributions to the long-range potential scaling as $1/R^3$ can be ignored because rotational states do not have dipole moments in the laboratory frame. Energy-exchange dipole-dipole contributions do not vanish in principle for $J = 0$ molecules, but can also be ignored by choosing atomic levels that do not allow the resonance conditions for energy transfer.

In this work, we report a large set of van der Waals C_6 coefficients that determine the long-range interaction between selected heteronuclear alkali-metal dimers (LiCs, RbCs, LiRb, and KRb) in their electronic and rovibrational ground state

*felipe.herrera.u@usach.cl

TABLE I. Parameters for the fitting $C_6 = \gamma_0 + \gamma_4 n^4 + \gamma_6 n^6 + \gamma_7 n^7$, for selected atom-molecule pairs involving ^{133}Cs atoms in Rydberg states n^2L_j, interacting with LiCs and RbCs molecules in the ground electronic and rovibrational state. $\Omega = m$ is the total angular momentum projection of the collision pair. C_6 is in atomic units (a_0^3). The fitting is accurate in the range $n = 40$–150. The notation $A[x]$ means $A \times 10^x$.

Molecule	L	j	$\lvert\Omega\rvert$	γ_0	γ_4	γ_6	γ_7
LiCs	S	1/2	1/2	1.518[11]	−1.035[5]	−30.94	0.1630
	P	1/2	1/2	2.104[12]	−1.984[6]	162.1	−1.606
		3/2	1/2	2.307[12]	−2.366[6]	238.2	−2.375
			3/2	2.149[12]	−2.186[6]	225.5	−2.236
	D	3/2	1/2	−1.428[12]	1.708[6]	−226.6	1.879
			3/2	−5.864[11]	7.756[5]	−134.4	1.090
		5/2	1/2	−1.431[12]	1.909[6]	−289.5	2.469
			3/2	−1.081[12]	1.462[6]	−234.1	1.973
			5/2	−3.809[11]	5.716[5]	−123.2	0.9800
RbCs	S	1/2	1/2	−2.907[10]	2.757[4]	−13.25	0.05058
	P	1/2	1/2	−3.542[11]	−1.737[5]	−3.808	−0.4723
		3/2	1/2	4.866[11]	−2.753[5]	18.15	−0.7826
			3/2	4.425[11]	−2.588[5]	19.43	−0.7408
	D	3/2	1/2	−3.906[11]	2.610[5]	−31.40	0.5847
			3/2	−2.156[11]	1.565[5]	−26.86	0.3579
		5/2	1/2	−4.818[11]	3.501[5]	−53.47	0.8316
			3/2	−3.846[11]	2.821[5]	−45.57	0.6657
			5/2	−1.901[11]	1.458[5]	−29.63	−0.3334

($^1\Sigma^+, v = 0, J = 0$) with ^{85}Rb and ^{133}Cs atoms in Rydberg states n^2L_j with $15 \leqslant n \leqslant 150$, taking into account spin-orbit coupling. n is the atomic principal quantum number, L is the atomic orbital angular momentum, j is the total electronic angular momentum, v is the vibrational quantum number of the molecule, and J is the rotational angular momentum. We focus on molecular [30–33] and Rydberg atom species [34,35] that are experimentally relevant. The precision of the computed C_6 coefficients is limited by the accuracy of the semiempirical quantum defects used.

We fit the computed atom-molecule C_6 coefficients as a function of n to a polynomial of the form

$$C_6 = \gamma_0 + \gamma_4 n^4 + \gamma_6 n^6 + \gamma_7 n^7, \tag{1}$$

which is valid in the range $40 \leqslant n \leqslant 150$. The accuracy of the fitting increases with n. We list the fitting coefficients for all the atom-molecule pairs considered in Table I for cesium and Table II for rubidium. The proposed n^7 scaling is consistent with the scaling of the static Rydberg state polarizability [36]. The data set of computed C_6 coefficients is provided in the Supplemental Material [37].

We describe in Sec. II the theoretical and numerical methodology used to compute C_6 coefficients. In Sec. III, we present the dispersion coefficients for selected atom-molecule pairs, and discuss their accuracy in Sec. IV. We conclude by discussing the possible implications of our results.

II. METHODOLOGY

In this section, we briefly review the theory of long-range interaction between a heteronuclear alkali-metal dimer (particle A) and an alkali-metal atom (particle B) in an arbitrary fine-structure level n^2L_j, in the absence of external static or electromagnetic fields. Our work extends the results in Refs. [27–29] to fine-structure states with high n, as relevant for Rydberg states.

A. Interaction potential

Consider the charge distributions of molecule A and atom B, separated by a distance larger than their corresponding LeRoy radii [26]. The long-range electrostatic interaction between a molecule (A) and atom (B) is given by the multipole expansion [38],

$$\hat{V}_{AB}(R) = \sum_{L_A=0}^{\infty}\sum_{L_B=0}^{\infty}\sum_{q=-L_<}^{L_<} \frac{f_{L_AL_Bq}}{R^{1+L_A+L_B}} \hat{Q}_q^{L_A}(\hat{r}_A)\hat{Q}_{-q}^{L_B}(\hat{r}_B), \tag{2}$$

where $L_<$ is the smallest of the integers L_A and L_B. The multipole moments $\hat{Q}_q^{L_X}(\hat{r}_X)$ associated with a particle $X = (A, B)$ can be written in spherical tensor form [39],

$$\hat{Q}_q^{L_X}(\hat{r}_X) = \left(\frac{4\pi}{2L_X+1}\right)^{1/2} \sum_i q_i \hat{r}_i^{L_X} Y_q^{L_X}(\theta_i, \varphi_i), \tag{3}$$

where q_i is the ith charge composing the X distribution and $Y_q^{L_X}(\theta_i, \varphi_i)$ is a spherical harmonics. Expectation values of the multipole moments depend on the electronic structure of the particle. For a two-particle coordinate system in which the quantization axis is pointing from the center of mass of particle A to the center of mass of particle B, the factor $f_{L_AL_Bq}$ in Eq. (2) becomes [29]

$$f_{L_AL_Bq} = \frac{(-1)^{L_B}(L_A+L_B)!}{\sqrt{(L_A+q)!(L_A-q)!(L_B+q)!(L_B-q)!}}. \tag{4}$$

B. Dispersion coefficients

In the long range, the interaction Hamiltonian $\hat{V}_{AB}(R)$ in Eq. (2) gives a perturbative correction to the asymptotic

TABLE II. Parameters for the fitting $C_6 = \gamma_0 + \gamma_4 n^4 + \gamma_6 n^6 + \gamma_7 n^7$, for selected atom-molecule pairs involving ^{85}Rb atoms in Rydberg states n^2L_j, interacting with RbCs, LiRb, and KRb molecules in the ground electronic and rovibrational state. $\Omega = m$ is the total angular momentum projection of the collision pair. C_6 is in atomic units (a_0^3). The fitting is accurate in the range $n = 40$–150. The notation $A[x]$ means $A \times 10^x$.

Molecule	L	j	$\lvert\Omega\rvert$	γ_0	γ_4	γ_6	γ_7
KRb	S	1/2	1/2	4.340[9]	−1905	−0.5274	4.695[−4]
	P	1/2	1/2	1.155[10]	27.48	−6.706	0.02190
		3/2	1/2	1.429[10]	−840.9	−7.419	0.02381
			3/2	1.227[10]	9.555	−7.089	0.02286
	D	3/2	1/2	4.907[9]	−3284	0.1596	−1.883[−3]
			3/2	6.531[9]	−2307	−2.039	6.199[−3]
		5/2	1/2	3.298[9]	−2486	0.4228	−2.302[−3]
			3/2	4.481[9]	−2337	−0.5691	1.173[−3]
			5/2	6.782[9]	−2026	−2.521	8.018[−3]
LiRb	S	1/2	1/2	1.381[11]	−1.085[5]	6.408	−0.04418
	P	1/2	1/2	5.353[11]	−4.224[5]	−13.06	0.01194
		3/2	1/2	6.063[11]	−4.839[5]	−12.77	1.718[−3]
			3/2	5.598[11]	−4.420[5]	−14.57	0.01386
	D	3/2	1/2	1.091[11]	−1.040[5]	11.58	−0.06377
			3/2	2.100[11]	−2.024[5]	3.214	−0.03349
		5/2	1/2	8.086[10]	−7.309[4]	10.89	−0.05510
			3/2	1.317[11]	−1.237[5]	7.670	−0.04539
			5/2	2.309[11]	−2.225[5]	1.254	−0.02591
RbCs	S	1/2	1/2	1.316[10]	−3897	−2.743	−7.242[−3]
	P	1/2	1/2	−1.576[10]	5.049[4]	−39.63	0.07148
		3/2	1/2	−1.225[10]	5.381[4]	−44.40	0.07713
			3/2	−1.640[10]	5.347[4]	−41.94	0.07316
	D	3/2	1/2	2.285[10]	−1.490[4]	1.265	−0.01663
			3/2	9.039[9]	7469	−12.55	0.01839
		5/2	3/2	5.808[10]	−1.796[4]	−1.099	−0.01126
			5/2	5.978[10]	−2261	−13.17	0.01667

energies of the collision partners. This energy shift is the interaction potential $V_{AB}(R)$, which can be evaluated using second-order degenerate perturbation theory to read [40,41]

$$V_{AB}(R) = \sum_n \frac{C_n}{R^n}, \tag{5}$$

where C_n are the dispersion coefficients. Values of C_n are obtained by defining the zeroth-order eigenstates of the collision pair. In the absence of external fields, these are given by product states of the form $|\Phi_{AB}^{(0)}\rangle = |\Psi_A^{(0)}\rangle\,|\Psi_B^{(0)}\rangle$, where in our case $|\Psi_A^{(0)}\rangle \equiv |X\,^1\Sigma^+\rangle\,|v = 0, J = 0\rangle$ is the absolute ground state of an alkali-metal dimer and $|\Psi_B^{(0)}\rangle \equiv |(n^2L)jm\rangle$ is a general fine-structure state of an alkali-metal atom, with m being the projection of the total electronic angular momentum along the quantization axis.

The nondegenerate rovibrational ground state of a $^1\Sigma$ molecule has a definite rotational angular momentum, and thus parity. Therefore, the lowest nonzero contribution to the expansion in Eq. (5) is C_6/R^6. For molecules in an excited rotational state $J \geqslant 1$, quadrupole moments can give nonvanishing C_5 coefficients [27–29]. In this work, we only consider the ground rotational state (i.e., $C_5 = 0$). The second-order atom-molecule dipole-dipole interaction thus leads to a C_6 coefficient of the form

$$\begin{aligned} C_6 = -4 \sum_{A'B'} & \frac{1}{\left(E_{A'}^{(0)} - E_A^{(0)}\right) + \left(E_{B'}^{(0)} - E_B^{(0)}\right)} \\ & \times \sum_{qq'} \left[\frac{\langle \Psi_A^{(0)} | \hat{Q}_q^{(1)} | \Psi_{A'}^{(0)} \rangle \langle \Psi_B^{(0)} | \hat{Q}_{-q}^{(1)} | \Psi_{B'}^{(0)} \rangle}{(1+q)!(1-q)!} \right. \\ & \left. \times \frac{\langle \Psi_{A'}^{(0)} | \hat{Q}_{-q'}^{(1)} | \Psi_A^{(0)} \rangle \langle \Psi_{B'}^{(0)} | \hat{Q}_{q'}^{(1)} | \Psi_B^{(0)} \rangle}{(1+q')!(1-q')!} \right], \end{aligned} \tag{6}$$

where $E_A^{(0)}$ and $E_B^{(0)}$ are the molecular and atomic asymptotic energies at $R \to \infty$. All projections of the dipole tensors $\hat{Q}_q^{(1)}$ are taken into account. Primed particle labels refer to intermediate states in the summation. Every intermediate rovibrational state $|\Psi_{A'}^{(0)}\rangle$ in ground and excited electronic potentials is taken into account, as explained below. M is the projection of the total angular momentum of the molecule along the internuclear axis. For alkali-metal atoms, we take into account all possible intermediate states $|\Psi_{B'}^{(0)}\rangle \equiv |(n'^2L')j'm'\rangle$ up to convergence of C_6.

Following Ref. [42], we rewrite the sum over states in Eq. (6) in a more convenient form using the identities

$$\frac{1}{a+b} = \frac{2}{\pi} \int_0^\infty d\omega \frac{ab}{(a^2+\omega^2)(b^2+\omega^2)} \tag{7}$$

and

$$\frac{1}{a-b}=\frac{2}{\pi}\int_0^\infty d\omega\frac{ab}{(a^2+\omega^2)(b^2+\omega^2)}+\frac{2a}{a^2-b^2}, \quad (8)$$

which hold for positive real parameters a and b. For molecular states, we set $a=E_{\gamma' v' J'}-E_{X\,^1\Sigma\, vJ}$, where γ' labels an intermediate electronic state. For atomic states, we set $b=E_{n'L'j'}-E_{nLj}$ for upward transitions ($E_{n'L'j'}>E_{nLj}$), and $b=E_{nLj}-E_{n'L'j'}$ for downward transitions ($E_{n'L'j'}<E_{nLj}$). Atom-molecule C_6 coefficients can thus be written as

$$C_6=-\sum_{q,q'}K(q,q')\Bigg\{\int_0^{\omega_{\rm cut}}\frac{d\omega}{2\pi}\,\alpha^{mm}_{-q-q'}(i\omega)\,\alpha^{MM}_{qq'}(i\omega) + \sum_{n''L''j''m''}\Theta(-\Delta E_{n''L''j''})\alpha^{MM}_{qq'}(\Delta E_{n''L''j''}) \times\mathcal{T}_{nLjm}(n''L''j''m'')\Bigg\}, \quad (9)$$

where $K(q,q')\equiv 4/[(1+q)!(1-q)!(1+q')!(1-q')!]$ and $\omega_{\rm cut}$ is a cutoff frequency.

The arguments of the integral in Eq. (9) are the dynamic atomic polarizability component $\alpha^{mm}_{-q-q'}(z)$ and the dynamic molecular polarizability component $\alpha^{MM}_{qq'}(z)$, each evaluated at the imaginary frequency $z=i\omega$. The second term in the curly bracket represents downward transitions in the atom, with $\Delta E_{n''L''j''}=E_{n''L''j''}-E_{nLj}$. The Heaviside function $\Theta(x)$ enforces the downward character of the transitions that contribute to this term. These terms are weighted by the product of the atomic transition dipole integrals,

$$\mathcal{T}_{nLjm}(n''L''j''m'')\equiv\langle(n^2L)jm|Q^{(1)}_{-q}|(n''^2L'')j''m''\rangle \times\langle(n''^2L'')j''m''|Q^{(1)}_{q'}|(n^2L)jm\rangle, \quad (10)$$

and the molecular polarizability function $\alpha^{MM}_{qq'}(\omega)$ evaluated at the frequency $\omega=\Delta E_{n''L''j''}/\hbar$. In this work, we evaluate both the integral and the downward contributions to C_6 up to convergence within a cutoff $\omega_{\rm cut}$, as described below in more detail.

C. Polarizability of atomic Rydberg states

The dynamic atomic polarizability $\alpha^{mm}_{-q-q}(\omega)$ in Eq. (9) can be written for a general atomic state $|k\rangle$ as

$$\alpha^{kk}_{pp'}(\omega)=\sum_l\frac{\langle k|\hat d^\dagger_p|l\rangle\,\langle l|\hat d_{p'}|k\rangle}{E_l-E_k-\omega}+\frac{\langle k|\hat d_{p'}|l\rangle\,\langle l|\hat d^\dagger_p|k\rangle}{E_l-E_k+\omega}, \quad (11)$$

where ω is the frequency of the dipolar response, $\hat d_p$ is the pth component of the electric dipole operator in the spherical basis, E_k is the zeroth-order energy of state $|k\rangle$, and the state summation runs over all other atomic states $|l\rangle$ in the spectrum, with $l\neq k$. For alkali-metal atoms, the relevant atomic states and energies are obtained by numerically solving the radial Schrödinger equation $[-\nabla^2/2+V_L(r)]\Phi_B(r)=E_{nLj}\Phi_B(r)$ with a pseudopotential $V_L(r)$ that describes the interaction of core electrons with a single valence electron at distance r from the core (origin), including spin-orbit coupling. The angular part of the atomic wave functions correspond to spherical harmonics $Y_{jm}(\theta,\phi)$. We solve for the radial wave function $\Phi_B(r)$ as in Ref. [43], with atomic energies given by $E_{nLj}=-hcR_\infty/(n-\delta_{nLj})^2$, where $hcR_\infty=1/2$ is the Rydberg constant (in atomic units). The fine-structure quantum defects δ_{nLj} used in this work are given in the Appendix, in terms of the Rydberg-Ritz coefficients for ^{85}Rb and ^{133}Cs atoms.

We use the atomic energies and radial wave functions to construct the sum over states in Eq. (11), for a desired atomic state $|(n^2L)jm\rangle$. For convenience, the angular parts of the dipole integrals are evaluated using angular momentum algebra [39]. The nonvanishing elements of the polarizability can thus be written as

$$\alpha^{mm}_{-q-q}(\omega)=\sum_{n''L''}\sum_{j''m''}(-1)^{2j''+2j-m''-m+q+1}\Bigg[\frac{2(E_{n''L''j''}-E_{nLj})}{(E_{n''L''j''}-E_{nLj})^2-\omega^2}(2j+1)(2L+1)(2j''+1)(2L''+1) \times\begin{pmatrix}L''&1&L\\0&0&0\end{pmatrix}^2\begin{Bmatrix}L&j&s\\j''&L''&1\end{Bmatrix}^2\begin{pmatrix}j''&1&j\\-m''&q&m\end{pmatrix}^2|\langle n''L''|er|nL\rangle|^2\Bigg], \quad (12)$$

where circular and curly brackets correspond to $3j$ and $6j$ symbols [39], respectively. We use Eq. (12) to compute the nonzero components of the polarizability tensor for atomic Rydberg states $|(n^2L)jm\rangle$ with $n\geqslant 15$, ensuring the convergence of the sum over intermediate states for each imaginary frequency $i\omega$ that is relevant in the evaluation of the C_6 integral in Eq. (9).

D. Polarizability of alkali-metal dimers

The dynamic molecular polarizability needed for the evaluation of the C_6 integral is also given by an expression as in Eq. (11), but for eigenstates $|k\rangle$ and energies E_k describing electronic, vibrational, and rotational state of alkali-metal dimers. For transition frequencies $(E_l-E_k)/\hbar$ up to near infrared ($\sim$1 THz), only states within the ground electronic potential need to be explicitly included in the summation. The contribution of transitions between rovibrational states in different electronic states is taken into account separately, as explained in what follows.

In the space-fixed frame, Eq. (11) can be given an explicit form by introducing molecular states $|\gamma,v,JM\rangle$ and energies $E_{\gamma vJ}$, where γ labels the electronic state. Molecular polarizability components for a rovibrational state $|X\,^1\Sigma,v,JM\rangle$ in the ground electronic state can thus be written as [44]

$$\alpha^{X\,^1\Sigma\,vJM}_{qq'}(\omega)=\sum_{\gamma'v'J'M'}\Bigg[\frac{2(-1)^q(E_{\gamma'v'J'}-E_{X\,^1\Sigma\,vJ})}{(E_{\gamma'v'J'}-E_{X\,^1\Sigma\,vJ})^2-\omega^2} \times\langle X\,^1\Sigma\,vJM|\hat Q^{(1)}_q|\gamma'v'J'M'\rangle \times\langle\gamma'v'J'M'|\hat Q^{(1)}_{-q'}|X\,^1\Sigma\,vJM\rangle\Bigg]. \quad (13)$$

As anticipated above, for transition frequencies up to the midinfrared, the dominant contributions to the molecular polarizability come from rovibrational transitions within the ground electronic state. Therefore, Eq. (13) can be rewritten as

$$\alpha_{qq'}^{X\,^1\Sigma\,vJM}(\omega) = \alpha_{qq'}^{\mathrm{rv}}(\omega) + \alpha_{qq'}^{\mathrm{el}}(\omega), \tag{14}$$

where $\alpha_{qq'}^{\mathrm{rv}}$ and $\alpha_{qq'}^{\mathrm{el}}$ are the rovibrational and electronic polarizabilities, respectively, given by

$$\alpha_{qq'}^{\mathrm{rv}}(\omega) = \sum_{v'J'M'} \left[\frac{2(-1)^q (E_{X\,^1\Sigma\,v'J'} - E_{X\,^1\Sigma\,vJ})}{(E_{X\,^1\Sigma\,v'J'} - E_{X\,^1\Sigma\,vJ})^2 - \omega^2} \times \langle X\,^1\Sigma\, vJM|\hat{Q}_q^{(1)}|X^1\Sigma v'J'M'\rangle \times \langle X^1\Sigma v'J'M'|\hat{Q}_{-q'}^{(1)}|X\,^1\Sigma\, vJM\rangle \right] \tag{15}$$

and

$$\alpha_{qq'}^{\mathrm{el}}(\omega) = \sum_{\gamma' \neq X\,^1\Sigma} \sum_{v'J'M'} \left[\frac{2(-1)^q (E_{\gamma' v'J'} - E_{X\,^1\Sigma\,vJ})}{(E_{\gamma' v'J'} - E_{X\,^1\Sigma\,vJ})^2 - \omega^2} \times \langle X\,^1\Sigma\, vJM|\hat{Q}_q^{(1)}|\gamma' v'J'M'\rangle \times \langle \gamma' v'J'M'|\hat{Q}_{-q'}^{(1)}|X\,^1\Sigma\, vJM\rangle \right]. \tag{16}$$

For evaluating the molecular dipole integrals in Eqs. (15) and (16), the space-fixed q component of the dipole operator is written in terms of the body-fixed p components through the unitary transformation $\hat{Q}_q^{(1)} = \sum_p \mathcal{D}_{qp}^{*(1)} \hat{Q}_p^{(1)}$, where $\mathcal{D}_{qp}^{*(1)}$ is an element of the Wigner rotation matrix [39]. Transforming to the molecule-fixed frame is convenient since the electronic and vibrational eigenfunctions are given in the body-fixed frame by most quantum chemistry packages. The nonvanishing terms of the rovibrational polarizability ($q' = q$) can thus be written as

$$\alpha_{qq}^{\mathrm{rv}}(\omega) = \sum_{v'J'M'} (2J+1)(2J'+1) \frac{2(E_{v'J'} - E_{vJ})}{(E_{v'J'} - E_{vJ})^2 - \omega^2} \times \begin{pmatrix} J' & 1 & J \\ 0 & 0 & 0 \end{pmatrix}^2 \begin{pmatrix} J' & 1 & J \\ -M' & -q & M \end{pmatrix}^2 \times \left| \langle vJ|\hat{Q}_0^{(1)}|v'J'\rangle \right|^2, \tag{17}$$

where a redundant electronic state label has been omitted. The nuclear dipole integrals $\langle vJ|\,\hat{Q}_0^{(1)}\,|v'J'\rangle$ can be evaluated directly once the rovibrational wave functions $|vJ\rangle$ are known. These are obtained by solving the corresponding nuclear Schrödinger equation (i.e., vibrations plus rotations) using a discrete variable representation (DVR) as in Ref. [45], with potential energy curves (PECs) and Durham expansions for the energies E_{vJ} given in Ref. [46] for the alkali-metal dimers used in this work.

For diatomic molecules, the electronic contribution to the polarizability in Eq. (14) is fully characterized in the body-fixed frame by the components $\alpha_{00}^{\mathrm{el}}(\omega)$ and $\alpha_{1,1}^{\mathrm{el}}(\omega) = \alpha_{-1,-1}^{\mathrm{el}}(\omega)$ [47], which define the parallel polarizability $\alpha_\parallel(\omega) = \alpha_{00}^{\mathrm{el}}(\omega)$ and the perpendicular polarizability $\alpha_\perp(\omega) = -\alpha_{\pm1,\pm1}^{\mathrm{el}}(\omega)$, with respect to its symmetry axis. For frequencies up to the near infrared, the dynamic electronic polarizability of alkali-metal dimers does not deviate significantly from their static values $\alpha_\parallel(0)$ and $\alpha_\perp(0)$. Accurate static electronic polarizabilities for several alkali-metal dimers can be obtained from Ref. [48]. Explicitly, the space-fixed polarizability tensor for alkali-metal dimers in the $^1\Sigma$ state is given by

$$\alpha_{qq}^{\mathrm{el}}(\omega) = \sum_{J'M'} (2J+1)(2J'+1) \begin{pmatrix} J' & 1 & J \\ -M' & -q & M \end{pmatrix}^2 \times \left[\begin{pmatrix} J' & 1 & J \\ 0 & 0 & 0 \end{pmatrix}^2 \alpha_\parallel + 2 \begin{pmatrix} J' & 1 & J \\ 1 & -1 & 0 \end{pmatrix}^2 \alpha_\perp \right]. \tag{18}$$

For the rovibrational ground state, Eq. (18) reduces to its isotropic value $\alpha_{\mathrm{iso}}^{\mathrm{el}} = (\alpha_\parallel + 2\alpha_\perp)/3$ for all q components. It was shown in Ref. [46] that for frequencies up to $\sim 10^3$ THz, the isotropic electronic molecular polarizability can be accurately approximated by

$$\alpha_{\mathrm{iso}}^{\mathrm{el}}(\omega) = \frac{2\omega_\Sigma\, d_\Sigma^2}{\omega_\Sigma^2 - \omega^2} + \frac{2\omega_\Pi\, d_\Pi^2}{\omega_\Pi^2 - \omega^2}, \tag{19}$$

where the parameters ω_Σ and d_Σ are the effective transition energy and dipole moment associated with the lowest $\Sigma \to \Sigma$ transition. The parameters ω_Π and d_Π are associated with the lowest $\Sigma \to \Pi$ transition. For the alkali-metal dimers used in this work, we take the parameters listed in Ref. [46] to estimate the electronic contribution to the molecular polarizability over the frequencies of interest.

Finally, we directly compute the downward transition terms that contribute to C_6 in Eq. (9) by evaluating the total molecular polarizability in Eq. (14) at the relevant atomic transition frequencies, with an explicit evaluation of the atomic dipole integrals in Eq. (10).

III. RESULTS

The theoretical framework described above can be used to obtain C_6 coefficients for any alkali-metal atom-molecule pair, provided the atomic quantum defects and the molecular polarizability are known. In this work, we restrict the analysis to atom-molecule pairs involving either ^{85}Rb or ^{133}Cs atoms, whose Rydberg levels have been widely studied [43]. For a given atom, we choose molecules that contain that specific atom in their structure. Such atom-molecule pairs can be expected to occur naturally in cotrapping experiments.

Specifically, we study the long-range interaction between two sets of collision partners: (i) ^{133}Cs Rydberg atoms interacting with LiCs and RbCs molecules, and (ii) ^{85}Rb Rydberg atoms interacting with KRb, LiRb, and RbCs molecules. We use Eq. (9) to compute the C_6 coefficient of each atom-molecule pair considered, as a function of the principal quantum number n of the atomic Rydberg state n^2L_j. We restrict our calculations to atomic states with $L \leqslant 2$.

The total angular momentum projection along the quantization axis,

$$\Omega = m + M, \tag{20}$$

is a conserved quantity for an atom-molecule collision. For molecules in the rovibrational ground state ($J = 0$), we thus have $\Omega = m$. Below we present C_6 coefficients for each

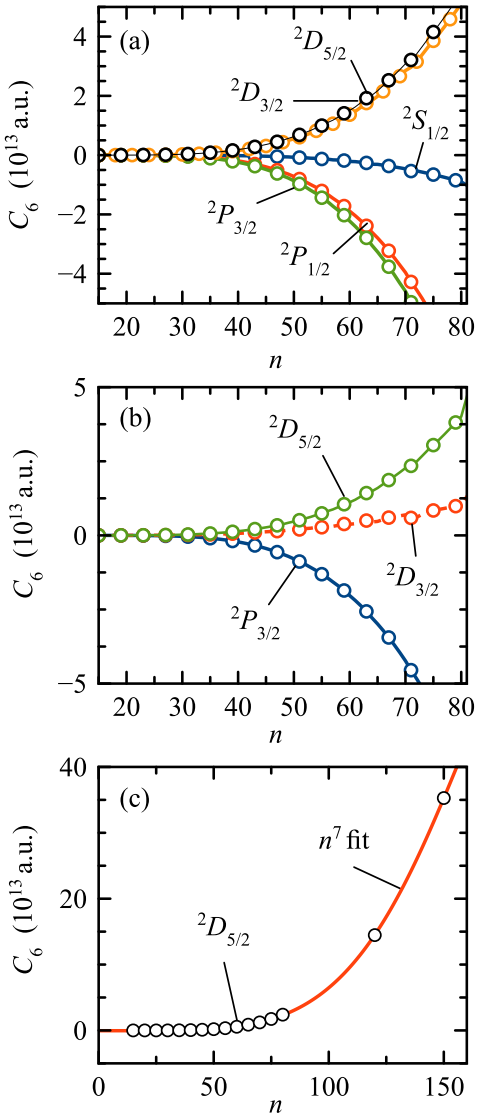

FIG. 1. C_6 dispersion coefficients as a function the atomic principal quantum number n for the Cs-LiCs collision pair. Results are shown for several atomic Rydberg states n^2L_j. LiCs is in the electronic and rovibrational ground state. Panels show results for different total angular momentum projections $\Omega = m + M$: (a) $|\Omega| = 1/2$, (b) $|\Omega| = 3/2$, (c) $|\Omega| = 5/2$. Solid lines correspond to a fitted n^7 scaling.

allowed value of $|\Omega|$. $C_6 < 0$ correspond to attractive interactions and $C_6 > 0$ describe repulsive potentials.

A. Cesium + molecule

In Fig. 1, we plot the C_6 coefficients for ^{133}Cs Rydberg states n^2L_j interacting with LiCs molecules in the rovibrational ground state, as a function of the atomic principal quantum number n, for all allowed values of Ω. For concreteness, we restrict the atomic quantum numbers to the range $15 \leqslant n \leqslant 150$, for $L \leqslant 2$.

For Cs Rydberg atoms in $^2S_{1/2}$, $^2P_{1/2}$, and $^2P_{3/2}$ states, the interaction with LiCs molecules is attractive over the entire range of n considered. As discussed in more detail below, this is due to the positive character of the atomic and molecular polarizability functions at imaginary frequencies $\alpha(i\omega)$, which determine the value of the integral term in Eq. (9). On the other hand, Cs atoms in $^2D_{3/2}$ and $^2D_{5/2}$ Rydberg states give rise to repulsive $1/R^6$ potentials. This repulsive character of the atom-molecule interaction is due to the predominantly negative atomic polarizability function $\alpha(i\omega)$, while the molecular polarizability function remains positive. This is consistent with n^2D Rydberg states having negative static polarizabilities $\alpha_{00}(\omega = 0)$ [49]. For both attractive and repulsive interactions, the magnitude of C_6 scales as $\sim n^7$ over a wide range of n, as shown explicitly in Fig. 1(c).

The C_6 coefficients for the Cs-RbCs collision pair exhibit the same qualitative behavior as the Cs-LiCs case, with repulsive potentials for ^2D_j states and attractive interaction for ^2S_j and ^2P_j Rydberg states. We provide the complete list of all C_6 coefficients computed for the Cs-LiCs and Cs-RbCs collision partners in the Supplemental Material [37].

B. Rubidium + molecule

In Fig. 2, we plot the C_6 coefficients for ^{85}Rb Rydberg states n^2L_j interacting with KRb molecules in the rovibrational ground state, as a function of the atomic principal quantum number n, for $L \leqslant 2$. The results resemble those of the Cs-LiCs pair with $^2S_{1/2}$, $^2P_{1/2}$, and $^2P_{3/2}$ atomic Rydberg states giving rise to attractive $1/R^6$ potentials that scale as $\sim n^7$, as show explicitly in Fig. 2(b) for $^2P_{3/2}$ states. In this case, ^2D_j states do not give repulsive potentials.

The C_6 coefficients for the interaction of Rb Rydberg atoms with RbCs and LiRb molecules exhibit the same qualitative behavior as the Rb-KRb case, giving attractive interaction for ^2S_j, ^2P_j, and ^2D_j Rydberg states. We provide the complete list of all C_6 coefficients computed for the Rb-KRb, Rb-LiRb, and Rb-RbCs collision partners in the Supplemental Material [37].

C. Scaling of C_6 with n

For all the atom-molecule pairs considered in this work, we fit the computed C_6 coefficients as a function of the atomic principal quantum number n to the polynomial,

$$C_6 = \gamma_0 + \gamma_4 n^4 + \gamma_6 n^6 + \gamma_7 n^7. \tag{21}$$

This scaling is valid in the range $n \approx 40$–150, with a fit quality that improves with increasing n. We list the fitting coefficients for Cs-LiCs and Cs-RbCs pairs in Table I for all of the considered atomic angular momentum states. The corresponding fitting coefficients for the collision pairs Rb-KRb, Rb-LiRb, and Rb-RbCs are given in Table II. The n^7 scaling found for C_6 is the same scaling of the static polarizability of Rydberg atoms [36]. This suggests that the long-range interaction potential is dominated by the giant Rydberg polarizability, as expected.

IV. DISCUSSION

Since the C_6 coefficients for the atom-molecule pairs listed in Tables I and II have yet to be experimentally measured, we estimate their accuracy from other considerations. The first question to address is the importance of the contribution to C_6 of the downward transition terms in Eq. (9). We find that for all of the considered atomic states n^2L_j, the downward

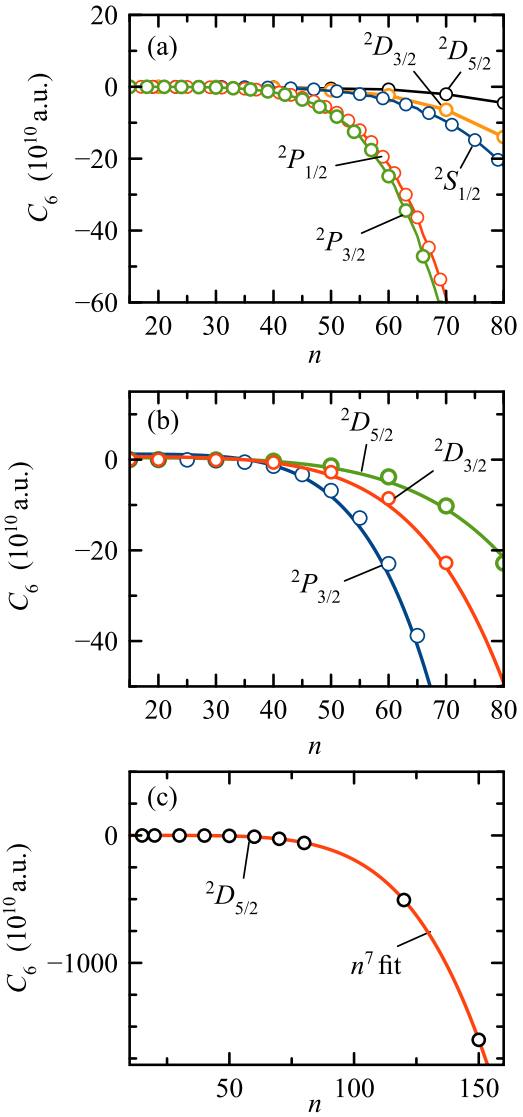

FIG. 2. C_6 dispersion coefficients as a function of the atomic principal quantum number n for the Rb-KRb collision pair. Results are shown for several atomic Rydberg states n^2L_j. KRb is in the electronic and rovibrational ground state. Panels show results for different total angular momentum projections $\Omega = m + M$: (a) $|\Omega| = 1/2$, (b) $|\Omega| = 3/2$, (c) $|\Omega| = 5/2$. Solid lines correspond to a fitted n^7 scaling.

transition terms represent a negligible contribution to C_6 in comparison with the integral term that involves the atomic Rydberg polarizability function.

This conclusion is valid provided we exclude resonant contributions to the downward transition term that involve evaluating the molecular polarizability at the atomic transition frequency $\Delta E_a = 2B_e$, where B_e is the rotational constant. High-n Rydberg states with transition frequencies that are resonant with rotational excitation frequencies may instead contribute to energy-exchange processes that scale as $1/R^3$, which can be avoided by careful selection of n and L quantum numbers. After removing resonant contributions ($\Delta E_a = 2B_e$) from the summation, the contribution of the integral term to C_6 in Eq. (9) was found to be at least three orders of magnitude

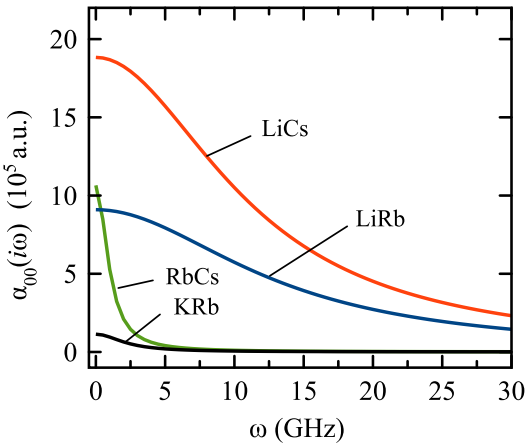

FIG. 3. Molecular polarizability function at imaginary frequency $\alpha_{00}(i\omega)$ for selected alkali-metal dimers in the electronic and rovibrational ground state $X\ ^1\Sigma^+$, $v = J = M = 0$.

larger than the contribution of the downward transition terms, for all the atom-molecule pairs studied in the range $n \geqslant 15$. One way to qualitatively understand this result is by comparing the n^7 scaling of the static atomic polarizability $\alpha(0)$ versus the n^2 scaling of the radial dipole integrals $\langle r^2\rangle^{1/2}$ for Rydberg states. The ratio between the integral (polarizability) and downward transitions (dipole) in Eq. (9) can thus scale at least as n^3, which gives a ratio of the order of 10^4 for $n = 50$ and 10^6 for $n = 100$.

A. Error bounds on C_6 values

After safely ignoring the atomic downward transition contributions to C_6 for $n > 15$, we now focus on estimating the accuracy of the frequency integral contribution to Eq. (9). The rovibrational structure and electrostatic response of most alkali-metal dimers in the ground $X\ ^1\Sigma$ state is well known from precision spectroscopy experiments and accurate *ab initio* studies [33,48,50]. Therefore, the molecular polarizability function α_{qq}^{JM} in Eq. (14) is assumed to be known with very high precision in comparison with the atomic polarizability function.[1] In Fig. 3, we plot the molecular polarizability function evaluated at imaginary frequencies $\alpha_{qq}^{JM}(i\omega)$ up to the microwave regime for KRb, RbCs, LiRb, and LiCs molecules. The figure shows the decreasing monotonic character of all of the studied molecular polarizability functions. As the frequency ω reaches the THz regime (not shown), all molecular functions $\alpha_{qq}^{JM}(i\omega)$ tend asymptotically to their isotropic static polarizabilities $\alpha_{\rm iso}^{\rm el}$ [Eq. (19)], and remain constant over a large frequency range up to several-hundred THz. In other words, over a broad frequency range up to ∼100 THz, the contribution of the molecular polarizability to C_6 in Eq. (9) is always positive and can be considered to be bounded from above by its static value.

The accuracy of our computed atomic polarizability functions $\alpha_{qq}^{mm}(i\omega)$ is limited by the precision of the quantum

[1]Our computed static molecular polarizabilities differ from the results in Ref. [46] by less than 2%.

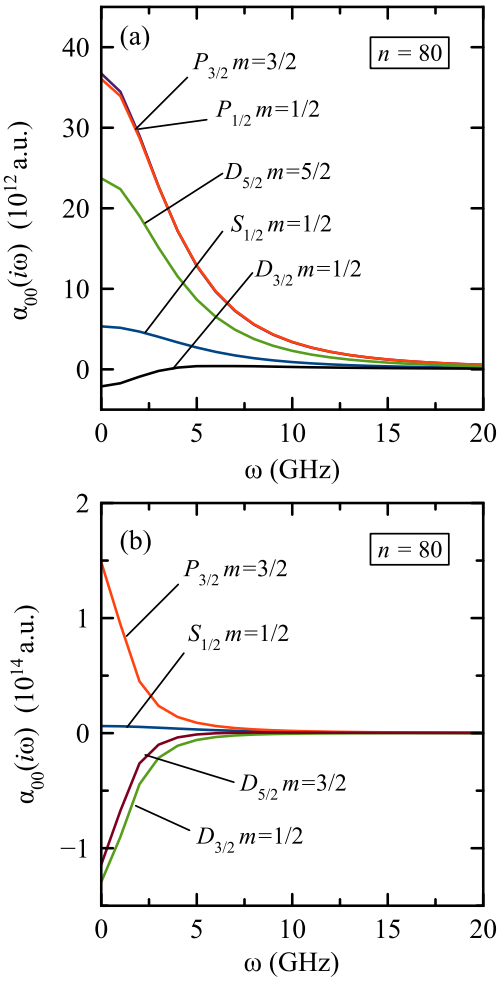

FIG. 4. Dynamic polarizability function at imaginary frequencies ($i\omega$) for (a) ^{85}Rb and (b) ^{133}Cs, for selected n^2L_j states with $n = 80$.

defects that are used, which we take from spectroscopic measurements [43]. For the considered atomic Rydberg states, the polarizability functions obtained from Eq. (12) are predominantly monotonic as a function of frequency, although we found specific states n^2L_j with nonmonotonic frequency dependence. We illustrate this in Fig. 4, where we show the polarizability functions $\alpha_{00}^{mm}(i\omega)$ for several n^2L_j Rydberg levels of Rb and Cs atoms in the $n = 80$ manifold. Figure 4(a) shows that for the projection $m = 1/2$ of the $80\,^2D_{3/2}$ Rydberg state of Rb, the function $\alpha(i\omega)$ is negative in the static limit, then has a maximum at $\omega \approx 6.5$ GHz, from where it decays to a positive asymptotic value up to a cutoff frequency $\omega_{\rm cut}$ of a few THz. This value at cutoff is five orders of magnitude smaller (not show) than the maximum in the microwave regime. In general, for all of the considered atomic states, we find that $|\alpha_{qq}^{mm}(i\omega)|$ is always bounded from above by its value at $\omega = 0$.

The error of the computed C_6 coefficients can thus be estimated for $n \geqslant 15$ as follows. Ignoring the downward transition terms and the error in the molecular polarizability function, Eq. (9) can be written as $\tilde{C}_6 = C_6 \pm \Delta C_6$, where $\tilde{C}_6$ is the dispersion coefficient obtained in our calculations and the error is approximately given by

$$\Delta C_6 \approx -\sum_{q,q'} \frac{K(q,q')}{2\pi} \int_0^{\omega_{\rm cut}} \frac{d\omega}{2\pi}\, \Delta\alpha_{qq'}^{mm}(i\omega)\, \alpha_{-q-q'}^{MM}(i\omega), \tag{22}$$

where $\Delta\alpha_{qq'}^{mm}(i\omega)$ is the error in the atomic polarizability function evaluated at imaginary frequencies. We can assume that the order of magnitude of C_6 and ΔC_6 is dominated by the 00 components of the atomic and molecular polarizability functions. If we also assume that the relative error $\Delta\alpha_{qq}^{mm}(i\omega)/\alpha_{qq}^{mm}(i\omega)$ remains constant over all frequencies up to the cutoff $\omega_{\rm cut}$, and use the fact that $|\alpha(i\omega)|$ is bounded from above by its static value in the atomic and molecular cases, we can estimate an approximate error bound for C_6 as

$$\left|\frac{\Delta C_6}{C_6}\right| \lesssim \left|\frac{\Delta\alpha_{00}^{mm}(0)}{\alpha_{00}^{mm}(0)}\right|. \tag{23}$$

In other words, the accuracy of our C_6 calculations cannot be expected to be better than the accuracy of the static atomic polarizability. The static polarizabilities of several Rydberg states of ^{85}Rb and ^{133}Cs are known from laser spectroscopy measurements in static electric fields [51–53], and also from precision calculations using state-of-the-art *ab initio* pseudopotentials [49]. Therefore, we can estimate $\Delta\alpha_{00}^{mm}(0)$ for several atomic Rydberg states n^2L_j by comparing with the available data. It proves convenient for comparisons to rewrite the atomic polarizability in Eq. (12) such that the Stark shift $\Delta E_{(nL)jm}$ of the Rydberg state $|(n^2L)jm\rangle$ in the presence of the electric field E in the Z direction can be written in the standard form [47],

$$\Delta E_{(nL)jm} = -\frac{1}{2}\left[\alpha_0(j) + \alpha_2(j)\frac{3m^2 - j(j+1)}{j(2j-1)}\right]E^2, \tag{24}$$

where $\alpha_0(j)$ is the scalar polarizability and $\alpha_2(j)$ is the tensor polarizability. The factor in square brackets is equal to $\alpha_{00}^{mm}(0)$ in Eq. (12).

In Fig. 5, we plot the the static polarizability of ^{133}Cs atoms in selected angular momentum states, as a function of the principal quantum number n. As a standard, we use *ab initio* results from Ref. [49]. Our computed values agree with the standard with very high accuracy. For example, the average relative errors over the range $15 \leqslant n \leqslant 50$ are -0.02% for $^2S_{1/2}$ states [Fig. 5(a)], $+0.27\,\%$ for $^2D_{5/2}$ states with $m = 5/2$ [Fig. 5(b)], and $+0.13\,\%$ for $^2D_{3/2}$ states with $m = 3/2$ [Fig. 5(c)]. For other Rydberg states of ^{133}Cs, we obtain similar accuracies.

In Fig. 6, we plot the the static polarizability of ^{85}Rb atoms in selected angular momentum states, as a function of n. For ^{85}Rb atoms, all the static polarizabilities that we compute show excellent agreement with reference values (errors smaller than 1%), except for the Rydberg state $n\,^2D_{3/2}$ with $m = 1/2$. For this atomic state, our results for $\alpha_{00}(0)$ have large relative errors around $n = 45$, as Fig. 6(c) shows. We can understand this by noting that for $j = 3/2$ and $m = 1/2$, Eq. (24) reads $\Delta E = -(\alpha_0 - \alpha_2)E^2/2$. For the $n\,^2D_{3/2}$ states of ^{85}Rb, experiments show that $\alpha_0 \approx \alpha_2$ in the range $n = 30$–60 [54], with $\alpha_0 \lesssim \alpha_2$ in the higher end of this range. This is confirmed by the *ab initio* results in Ref. [49], which predict a change of sign in the static polarizability at $n = 46$, from

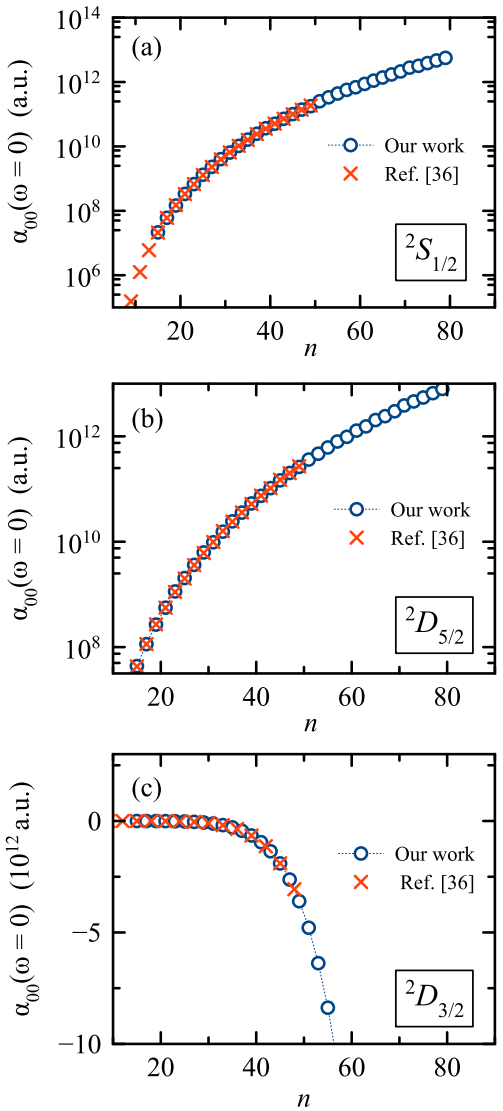

FIG. 5. Static polarizability of ^{133}Cs atoms in selected angular momentum states (in units of a_0^3), as a function of the principal quantum number n, for ^{133}Cs atoms in selected angular momentum states: (a) α_{00} component for $^2S_{1/2}$, (b) α_{00} component for $^2D_{5/2}$, $m = 5/2$, (c) α_{00}, α_{11}, and α_{-1-1} components for $^2D_{3/2}$ $m = 1/2$. Results for α_{00} from Ref. [49] are also shown.

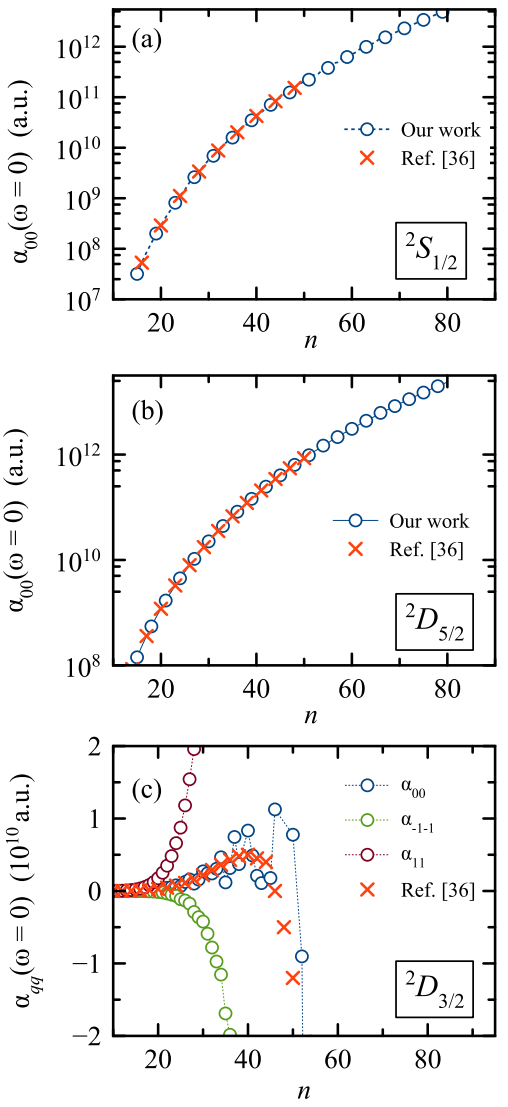

FIG. 6. Static polarizability of ^{85}Rb atoms in selected angular momentum states (in units of a_0^3), as a function of the principal quantum number n: (a) α_{00} component for $^2S_{1/2}$, (b) α_{00} component for $^2D_{5/2}$, $m = 5/2$, (c) α_{00}, α_{11}, and α_{-1-1} components for $^2D_{3/2}$ $m = 1/2$. Results for α_{00} from Ref. [49] are also shown.

positive to negative. By separately comparing our results with experimental and theoretical values for α_0 and α_2 (not shown), we observe that our errors are of the same magnitude as the difference $\alpha_0 - \alpha_2$ in the range $30 < n < 60$, which makes the atomic polarizability calculations unreliable for this particular tensor component (α_{00}) and atomic quantum numbers. Errors can be traced to the empirical quantum defects that are used. We also show in Fig. 6(c) that over the same range of n in which $\alpha_{00}(0)$ exhibits large relative errors, other polarizability components that do not change sign behave smoothly.

Another possible source of error in our C_6 calculations is the choice of the high-frequency cutoff $\omega_{\rm cut}$ in the numerical integration of Eq. (9). For every atomic Rydberg state that is considered, we tested the numerical convergence of the integration by increasing the value of the cutoff until the relative change $\delta C_6/C_6$ was smaller than a predefined tolerance value ε. For atom-molecule pairs involving both ^{85}Rb and ^{133}Cs atoms, the polarizability integral converges faster with increasing cutoff for intermediate and high values of $n \gtrsim 30$, in comparison with low-n states. The latter result in slower integral convergence. We converged all our $n \approx 15$ integrals at $\omega_{\rm cut} = 3$ THz with a tolerance $\varepsilon = 0.01$, which ensures convergence over an entire range of n.

B. Effect of the molecular dipole moment

In Fig. 7, we show the increase in the magnitude of C_6 as the permanent dipole moment of alkali-metal dimers increases, for selected states $n\,^2P_{1/2}$ of ^{85}Rb. The C_6 coefficient for the Rb-LiRb pair is larger than the corresponding values for RbCs and KRb, which have a smaller dipole moment. The

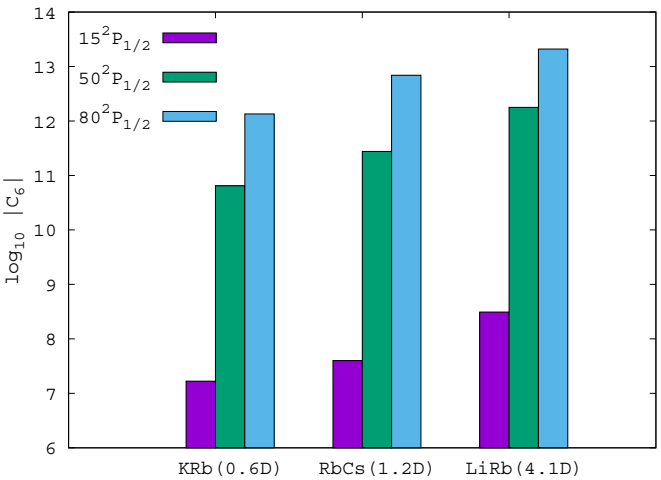

FIG. 7. Bar plots $\log_{10}|C_6|$ for $n = 15, 50, 80$ for atom-molecule pairs involving ^{85}Rb atoms in the $n\,^2P_{1/2}$ state with KRb, RbCs, and LiRb molecules in the rovibrational ground state. The permanent dipole moment of each molecule is shown in parentheses on the horizontal axis [48].

same trend also holds for other n^2L_j states of ^{85}Rb, and for atom-molecule pairs involving ^{133}Cs atoms.

V. CONCLUSION

The characteristic length scale for the van der Waals interaction between a Rydberg atom and a ground-state alkali-metal dimer is the LeRoy radius $R_{\rm LR}$ [26], given by the average root-mean-square electron radius of the collision pair. For alkali-metal atoms in low-lying Rydberg states ($n \approx 15$–20), the typical mean atomic radius can be of the order of 100–1000 a_0, where a_0 is the Bohr radius, thus exceeding by orders the typical size of the electron radius of ground-state molecules of only a few Bohr radii. The ratio between atomic and molecular radial distances further increases with n. For the atomic states that are considered in this work, the van der Waals length is thus dominated by the LeRoy radius of the Rydberg atom, $R_{nL} \equiv \langle n^2L|r^2|n^2L\rangle^{1/2}$. Given the n^2 scaling of the Rydberg radius and the n^7 scaling of the atom-molecule C_6 coefficients, the van der Waals energy should thus approximately scale as $U_{\rm vdW} \equiv C_6/R_{nL}^6 \sim n^{-5}$. We find this scaling to be most accurate for $n \gtrsim 50$.

From the values of C_6 listed in Tables I and II, the van der Waals energy $U_{\rm vdW}$ can be estimated in absolute units. For example, for the LiCs–Cs system with ^{133}Cs in the $n\,^2D_{5/2}$ state and $\Omega = 5/2$, the van der Waals potential is repulsive [Fig. 1(c)], with a collisional barrier reaching $U_{\rm vdW} \approx 38$ MHz for $n = 20$. This should be sufficient to avoid short-range collisions for atom-molecule pairs with relative kinetic energy up to 1.82 mK. By increasing the atomic quantum number to $n = 40$, the potential barrier drops to $U_{\rm vdW} \approx 0.43$ MHz for the same collision pair. Our results thus suggest that given a specific atom-molecule system of experimental interest, it is possible to find an atomic Rydberg state that gives an attractive or repulsive potential with a desired interaction strength.

TABLE III. Rydberg-Ritz coefficients for ^{85}Rb.

L_j	a	b	c	d	$n_{\rm min}$
$S_{1/2}$	3.1311804(10)	0.1784(6)	−1.8		14
$P_{1/2}$	2.6548849(10)	0.2900(6)	−7.9040	116.4373	11
$P_{3/2}$	2.6416737(10)	0.2950(7)	−0.97495	14.6001	13
$D_{3/2}$	1.34809171(40)	−0.60286(26)	−1.50517	−2.4206	4
$D_{5/2}$	1.34646572(30)	−0.59600(18)	−1.50517	−2.4206	4
F_j	0.016312	−0.064007	−0.36005	3.2390	4

We can extend the formalism in this work to also obtain van der Waals coefficients for excited rovibrational states of alkali-metal dimers. In this case, C_5 coefficients do not vanish in general [29]. The interplay between C_5 and C_6 with opposite signs at long distances can possibly lead to long-range potential wells that can support Rydberg-like metastable bound states accessible in photoassociation spectroscopy [4,27–29].

Repulsive van der Waals interactions may be used for sympathetic cooling of alkali-metal dimers via elastic collisions with ultracold Rydberg atoms. Since inelastic and reactive ultracold collisions [55,56] can lead to spontaneously emitted photons carrying energy away from a trapped system [23], it should be possible to measure the elastic-to-inelastic scattering rates and follow the thermalization process of a cotrapped atom-molecule mixture. Attractive van del Waals potentials can be exploited to form long-range alkali-metal trimers via photoassociation [7].

ACKNOWLEDGMENTS

F.H. is thankful for support from ANID through REDES ETAPA INICIAL Convocatoria 2017 Grant No. REDI170423 and Fondecyt Regular Grant No. 1181743. V.O. and F.H. are supported by Iniciativa Científica Milenio (ICM) through the Millennium Institute for Research in Optics (MIRO).

APPENDIX: QUANTUM DEFECTS

The quantum defects used in this work are collected from Ref. [43] in terms of the expansion

$$\delta_{nLj} = a + \frac{b}{(n-a)^2} + \frac{c}{(n-a)^2} + \frac{d}{(n-a)^2} + \frac{e}{(n-a)^2}, \tag{A1}$$

where the Rydberg-Ritz coefficients (a, b, c, d) are given in Table III for ^{85}Rb and Table IV for ^{133}Cs atoms, together with the minimum value of n for which the expansion is estimated to be valid.

TABLE IV. Rydberg-Ritz coefficients for ^{133}Cs.

L_j	a	b	c	d	$n_{\rm min}$
$S_{1/2}$	4.049352(38)	0.238(7)	0.24044	0.12177	6
$P_{1/2}$	3.5916(5)	0.36(1)	0.34284	1.23986	6
$P_{3/2}$	3.5590(7)	0.38(1)	0.28013	1.57631	6
$D_{3/2}$	2.475454(20)	0.010(4)	−0.43324	−0.96555	5
$D_{5/2}$	2.466308(30)	0.015(6)	−0.43674	−0.74442	5
$F_{5/2}$	0.033587	−0.213732	0.70025	−3.66216	4

[1] M. Saffman, T. G. Walker, and K. Mølmer, Quantum information with Rydberg atoms, Rev. Mod. Phys. **82**, 2313 (2010).

[2] T. Peyronel, O. Firstenberg, Q.-Y. Liang, S. Hofferberth, A. V. Gorshkov, T. Pohl, M. D. Lukin, and V. Vuletić, Quantum nonlinear optics with single photons enabled by strongly interacting atoms, Nature (London) **488**, 57 (2012).

[3] A. Facon, E.-K. Dietsche, D. Grosso, S. Haroche, J.-M. Raimond, M. Brune, and S. Gleyzes, A sensitive electrometer based on a Rydberg atom in a Schrödinger-cat state, Nature (London) **535**, 262 (2016).

[4] J. Pérez-Ríos, M. Lepers, and O. Dulieu, Theory of Long-Range Ultracold Atom-Molecule Photoassociation, Phys. Rev. Lett. **115**, 073201 (2015).

[5] C. H. Greene, A. S. Dickinson, and H. R. Sadeghpour, Creation of Polar and Nonpolar Ultra-Long-Range Rydberg Molecules, Phys. Rev. Lett. **85**, 2458 (2000).

[6] V. Bendkowsky, B. Butscher, J. Nipper, J. P. Shaffer, R. Löw, and T. Pfau, Observation of ultralong-range Rydberg molecules, Nature (London) **458**, 1005 (2009).

[7] J. P. Shaffer, S. T. Rittenhouse, and H. R. Sadeghpour, Ultracold Rydberg molecules, Nat. Commun. **9**, 1965 (2018).

[8] M. T. Eiles, H. Lee, J. Pérez-Ríos, and C. H. Greene, Anisotropic blockade using pendular long-range rydberg molecules, Phys. Rev. A **95**, 052708 (2017).

[9] P. J. J. Luukko and J.-M. Rost, Polyatomic Trilobite Rydberg Molecules in a Dense Random Gas, Phys. Rev. Lett. **119**, 203001 (2017).

[10] T. C. Liebisch, M. Schlagmüller, F. Engel, H. Nguyen, J. Balewski, G. Lochead, F. Böttcher, K. M. Westphal, K. S. Kleinbach, T. Schmid, A. Gaj, R. Löw, S. Hofferberth, T. Pfau, J. Pérez-Ríos, and C. H. Greene, Controlling Rydberg atom excitations in dense background gases, J. Phys. B: At., Mol. Opt. Phys. **49**, 182001 (2016).

[11] A. A. Kamenski, N. L. Manakov, S. N. Mokhnenko, and V. D. Ovsiannikov, Energy of van der Waals and dipole-dipole interactions between atoms in Rydberg states, Phys. Rev. A **96**, 032716 (2017).

[12] I. Mourachko, D. Comparat, F. de Tomasi, A. Fioretti, P. Nosbaum, V. M. Akulin, and P. Pillet, Many-Body Effects in a Frozen Rydberg Gas, Phys. Rev. Lett. **80**, 253 (1998).

[13] H. Bernien, S. Schwartz, A. Keesling, H. Levine, A. Omran, H. Pichler, S. Choi, A. S. Zibrov, M. Endres, M. Greiner, V. Vuletić, and M. D. Lukin, Probing many-body dynamics on a 51-atom quantum simulator, Nature (London) **551**, 579 (2017).

[14] C. J. Turner, A. A. Michailidis, D. A. Abanin, M. Serbyn, and Z. Papić, Weak ergodicity breaking from quantum many-body scars, Nat. Phys. **14**, 745 (2018).

[15] C. J. Turner, A. A. Michailidis, D. A. Abanin, M. Serbyn, and Z. Papić, Quantum scarred eigenstates in a rydberg atom chain: Entanglement, breakdown of thermalization, and stability to perturbations, Phys. Rev. B **98**, 155134 (2018).

[16] W. R. Anderson, J. R. Veale, and T. F. Gallagher, Resonant Dipole-Dipole Energy Transfer in a Nearly Frozen Rydberg Gas, Phys. Rev. Lett. **80**, 249 (1998).

[17] D. Comparat and P. Pillet, Dipole blockade in a cold Rydberg atomic sample, J. Opt. Soc. Am. B **27**, A208 (2010).

[18] G. Vitrant, J. M. Raimond, M. Gross, and S. Haroche, Rydberg to plasma evolution in a dense gas of very excited atoms, J. Phys. B **15**, L49 (1982).

[19] T. C. Killian, S. Kulin, S. D. Bergeson, L. A. Orozco, C. Orzel, and S. L. Rolston, Creation of an Ultracold Neutral Plasma, Phys. Rev. Lett. **83**, 4776 (1999).

[20] M. P. Robinson, B. Laburthe Tolra, Michael W. Noel, T. F. Gallagher, and P. Pillet, Spontaneous Evolution of Rydberg Atoms into an Ultracold Plasma, Phys. Rev. Lett. **85**, 4466 (2000).

[21] F. Jarisch and M. Zeppenfeld, State resolved investigation of Förster resonant energy transfer in collisions between polar molecules and Rydberg atoms, New J. Phys. **20**, 113044 (2018).

[22] M. Zeppenfeld, Nondestructive detection of polar molecules via Rydberg atoms, Europhys. Lett. **118**, 13002 (2017).

[23] B. Zhao, A. W. Glaetzle, G. Pupillo, and P. Zoller, Atomic Rydberg Reservoirs for Polar Molecules, Phys. Rev. Lett. **108**, 193007 (2012).

[24] S. D. Huber and H. P. Büchler, Dipole-Interaction-Mediated Laser Cooling of Polar Molecules to Ultracold Temperatures, Phys. Rev. Lett. **108**, 193006 (2012).

[25] K.-K. Ni, S. Ospelkaus, D. Wang, G. Quéméner, B. Neyenhuis, M. H. G. de Miranda, J. L. Bohn, J. Ye, and D. S. Jin, Dipolar collisions of polar molecules in the quantum regimes, Nature (London) **464**, 1324 (2010).

[26] R. J. Le Roy, Theory of deviations from the limiting near-dissociation behavior of diatomic molecules, J. Chem. Phys. **73**, 6003 (1980).

[27] M. Lepers and O. Dulieu, Long-range interactions between ultracold atoms and molecules including atomic spin–orbit, Phys. Chem. Chem. Phys. **13**, 19106 (2011).

[28] M. Lepers, R. Vexiau, N. Bouloufa, O. Dulieu, and V. Kokoouline, Photoassociation of a cold-atom-molecule pair. ii. Second-order perturbation approach, Phys. Rev. A **83**, 042707 (2011).

[29] M. Lepers, O. Dulieu, and V. Kokoouline, Photoassociation of a cold-atom–molecule pair: Long-range quadrupole-quadrupole interactions, Phys. Rev. A **82**, 042711 (2010).

[30] K.-K. Ni, S. Ospelkaus, M. H. G. de Miranda, A. Pe'er, B. Neyenhuis, J. J. Zirbel, S. Kotochigova, P. S. Julienne, D. S. Jin, and J. Ye, A high phase-space-density gas of polar molecules, Science **322**, 231 (2008).

[31] D. B. Blasing, I. C. Stevenson, J. Pérez-Ríos, D. S. Elliott, and Y. P. Chen, Short-range photoassociation of lirb, Phys. Rev. A **94**, 062504 (2016).

[32] P. K. Molony, P. D. Gregory, Zhonghua Ji, Bo Lu, M. P. Köppinger, C. Ruth Le Sueur, C. L. Blackley, J. M. Hutson, and S. L. Cornish, Creation of Ultracold ^{87}Rb ^{133}Cs Molecules in the Rovibrational Ground State, Phys. Rev. Lett. **113**, 255301 (2014).

[33] J. Deiglmayr, A. Grochola, M. Repp, K. Mortlbauer, C. Gluck, J. Lange, O. Dulieu, R. Wester, and M. Weidemuller, Formation of Ultracold Polar Molecules in the Rovibrational Ground State, Phys. Rev. Lett. **101**, 133004 (2008).

[34] M. A. Bellos, R. Carollo, J. Banerjee, E. E. Eyler, P. L. Gould, and W. C. Stwalley, Excitation of Weakly Bound Molecules to Trilobitelike Rydberg States, Phys. Rev. Lett. **111**, 053001 (2013).

[35] D. Booth, S. T. Rittenhouse, J. Yang, H. R. Sadeghpour, and J. P. Shaffer, Production of trilobite Rydberg molecule dimers with Kilo-Debye permanent electric dipole moments, Science **348**, 99 (2015).

[36] T. F. Gallagher, *Rydberg Atoms* (Cambridge University Press, Cambridge, 1994).

[37] See Supplemental Material at http://link.aps.org/supplemental/10.1103/PhysRevA.101.032705 for a data set with the C_6 coefficients (a.u.) as a function of the atomic principal quantum number n, for each of the atom-molecule pairs listed in Tables I and II of the main text. See the README file for more details.

[38] M. R. Flannery, D. Vrinceanu, and V. N. Ostrovsky, Long-range interaction between polar Rydberg atoms, J. Phys. B: At., Mol. Opt. Phys. **38**, S279 (2005).

[39] R. N. Zare, *Angular Momentum* (Wiley, New York, 1988).

[40] M. Marinescu, H. R. Sadeghpour, and A. Dalgarno, Dispersion coefficients for alkali-metal dimers, Phys. Rev. A **49**, 982 (1994).

[41] M. Marinescu and A. Dalgarno, Dispersion forces and long-range electronic transition dipole moments of alkali-metal dimer excited states, Phys. Rev. A **52**, 311 (1995).

[42] D. Spelsberg, T. Lorenz, and W. Meyer, Dynamic multipole polarizabilities and long range interaction coefficients for the systems H, Li, Na, K, He, H^-, H_2, Li_2, Na_2, and K_2, J. Chem. Phys. **99**, 7845 (1993).

[43] K. Singer, Ph.D. thesis, Interactions in an ultracold gas of Rydberg atoms, University of Freiburg, 2004.

[44] F. Herrera, Ph.D. thesis, Quantum control of binary and many-body interactions in ultracold molecular gases, University of British Columbia, 2012.

[45] D. T. Colbert and W. H. Miller, A novel discrete variable representation for quantum mechanical reactive scattering via the s-matrix Kohn method, J. Chem. Phys. **96**, 1982 (1992).

[46] R. Vexiau, D. Borsalino, M. Lepers, A. Orbán, M. Aymar, O. Dulieu, and N. Bouloufa-Maafa, Dynamic dipole polarizabilities of heteronuclear alkali dimers: optical response, trapping and control of ultracold molecules, Int. Rev. Phys. Chem. **36**, 709 (2017).

[47] K. D. Bonin and V. V. Kresin, *Electric-dipole Polarizabilities of Atoms, Molecules and Clusters* (World Scientific, Singapore, 1997).

[48] J. Deiglmayr, M. Aymar, R. Wester, M. Weidemuller, and O. Dulieu, Calculations of static dipole polarizabilities of alkali dimers: Prospects for alignment of ultracold molecules, J. Chem. Phys. **129**, 064309 (2008).

[49] V. A. Yerokhin, S. Y. Buhmann, S. Fritzsche, and A. Surzhykov, Electric dipole polarizabilities of rydberg states of alkali-metal atoms, Phys. Rev. A **94**, 032503 (2016).

[50] J. Deiglmayr, M. Repp, R. Wester, O. Dulieu, and M. Weidemüller, Inelastic collisions of ultracold polar lics molecules with caesium atoms in an optical dipole trap, Phys. Chem. Chem. Phys. **13**, 19101 (2011).

[51] M. L. Zimmerman, M. G. Littman, M. M. Kash, and D. Kleppner, Stark structure of the Rydberg states of alkali-metal atoms, Phys. Rev. A **20**, 2251 (1979).

[52] M. S. O'Sullivan and B. P. Stoicheff, Scalar and tensor polarizabilities of ^2d Rydberg states in Rb, Phys. Rev. A **33**, 1640 (1986).

[53] J. Zhao, H. Zhang, Z. Feng, X. Zhu, L. Zhang, C. Li, and S. Jia, Measurement of polarizability of cesium nd state in magneto-optical trap, J. Phys. Soc. Jpn. **80**, 034303 (2011).

[54] Zhangli Lai, Shichao Zhang, Qingdong Gou, and Yong Li, Polarizabilities of Rydberg states of Rb atoms with n up to 140, Phys. Rev. A **98**, 052503 (2018).

[55] P. S. Julienne, Ultracold molecules from ultracold atoms: A case study with the KRb molecule, Faraday Discuss. **142**, 361 (2009).

[56] Z. Idziaszek and P. S. Julienne, Universal Rate Constants for Reactive Collisions of Ultracold Molecules, Phys. Rev. Lett. **104**, 113202 (2010).